IEEE Access
Multidisciplinary ⋮ Rapid Review ⋮ Open Access Journal

Received June 13, 2020, accepted July 1, 2020, date of publication July 6, 2020, date of current version July 17, 2020.

Digital Object Identifier 10.1109/ACCESS.2020.3007465

A New Method for Segmentation of the Coronary Arteries of Interest and Diameter Measurement

LURONG JIANG[1], YUE LI[1], JIANWEI PAN[2], DANHUA ZHU[3], JIJUN TONG[1], AND TING SHU[1]

[1]School of Information Science and Technology, Zhejiang Sci-Tech University, Hangzhou 310018, China
[2]Department of Neurosurgery, First Affiliated Hospital, School of Medicine, Zhejiang University, Hangzhou 310011, China
[3]State Key Laboratory for Diagnosis and Treatment of Infectious Diseases, National Clinical Research Center for Infectious Diseases, National Medical Center for Infectious Diseases, Collaborative Innovation Center for Diagnosis and Treatment of Infectious Diseases, First Affiliated Hospital, College of Medicine, Zhejiang University, Hangzhou 310018, China

Corresponding author: Jijun Tong (jijuntong@zstu.edu.cn)

This work was supported in part by the National Natural Science Foundation of China under Grant 61602417 and Grant 81971688, in part by the Zhejiang Provincial Key Research and Development Plan under Grant 2015C03023, in part by the Zhejiang Provincial Natural Science Foundation of China under Grant LY17F020033, in part by the Public Welfare Project of Zhejiang Province under Grant 2014C33102, in part by the Fundamental Scientific Research Project of Zhejiang Sci-Tech University (ZSTU) under Grant 2019Q042 and Grant 2019Q039, and in part by the 521 Talent Project of ZSTU.

ABSTRACT Cardiovascular disease is a severe threat to human health. The assessment of the degree of cardiovascular stenosis is very important for the diagnosis of cardiovascular disease. The segmentation of coronary angiographic images is the basis of analyzing the degree of stenosis. In this paper, a method that evaluates explicitly the degree of stenosis of blood vessels of interest is proposed. This method first extracts the vessels of interest by interactive segmentation, then thins it, and then calculates the diameter by edge intersection method. The average Dice Similarity Coefficient (DSC) value of the proposed segmentation method exceeds 92%, and the average Jaccard Similarity (JAC) value is over 86%. The area under the ROC curve value of the method is larger than the u-net method and the multiscale Hessian method. The results indicate that the interactive method can have good segmentation results and meet the general segmentation requirements. The qualitative and quantitative evaluation of the diameter measurement effect also shows that the effect of the corresponding diameter measurement method can reflect the change of the thickness of the blood vessel and basically meet the needs of clinical use.

INDEX TERMS Coronary angiography, vessel segmentation, diameter measurement, thinning algorithm.

I. INTRODUCTION

Cardiovascular disease (CVD) has become the leading cause of human health hazards and death [1]. With the deepening of the population aging, the prevalence of cardiovascular disease in the world has also increased year by year. Coronary heart disease (CHD) has the highest incidence due to coronary artery stenosis, obstruction, and insufficient blood supply. Detection of coronary artery disease such as atherosclerosis or stenosis in the early stage of cardiovascular disease is of great significance for the early treatment and intervention of coronary heart disease.

Coronary angiography (CAG) can reveal the anatomical deformity of coronary arteries and the location, degree, and scope of obstructive lesions. It is currently a widely accepted method that can directly observe the morphology of coronary arteries [2]. The most significant feature of CAG is visualization, and it is easier to judge the degree of blood vessel stenosis.

In order to quantitatively assess the degree of stenosis of blood vessels, it is necessary to perform segmentation operations on the obtained CAG images to segment the blood vessels. The segmentation of blood vessels in angiographic images has been studied and summarized by many researchers [3]–[5]. Due to the low contrast between the blood vessel and the background in the CAG image, the image may contain noise, changes in vessel thickness, bifurcations, and crossings, etc. It is difficult to get the blood vessel segment accurately. Some pre-processing operations are often used before segmentation for a better effect. We divide the segmentation methods of CAG image into several methods: traditional image processing methods, deformable model methods, tracking methods, graph-based methods, and deep learning.

The associate editor coordinating the review of this manuscript and approving it for publication was Essam A. Rashed.

Traditional image processing methods can be divided into several different methods: thresholding method, region growing method, statistical region merging method, and matched filter. Lian *et al.* [6] used an iterative threshold-based method to extract deformed parts of blood vessels. They first segmented the image into several sub-images and divided these sub-images into two different categories using the maximum inter-class variance method. The gray average and median values are continuously iterated. Cruz-Aceves *et al.* [7] used a multi-objective threshold method to binarize the amplitude of the multi-scale Gabor filter to segment the blood vessel. Wang *et al.* [8] first performed multi-scale Hessian enhancement, based on multiple seed points for regional growth, which can connect non-continuous vascular segments, which is better than the single seed point enhancement method. Kulathilake *et al.* [9] used mathematical morphology and flood filling methods to achieve regional growth operations. They finally extracted the blood vessel edges from the marked blood vessel structures. Kerkeni *et al.* [10] performed multi-scale Hessian enhancement before the segmentation. The regional growth operation they use was based on different scales. They set growth rules taking into account different scales. Statistical region merging was first proposed by Nock and Nielsen [11] in 2004. This method regards the gray value of pixels in the image as a statistical model to judge the similarity between adjacent pixels. Wan *et al.* [12] used 4-neighborhood statistical region merging method to segment the target pixels after the multi-scale Hessian enhancement. The matched filter is a method to complete target extraction by convolving the image with various matched filters [13]. Cruz-Aceves *et al.* [14] proposed a multi-scale Gaussian matched filter based on neural networks, which can detect blood vessels of different scales.

The deformable model defines the target (usually a surface or a curve) as an initial model, which will gradually deform under the action of internal and external forces. Deformable model methods can be divided into edge-based and region-based. Among the edge-based methods, the snake model [15] and the level set method [16] are widely used. Devi and Kumaravel [17] provided a new external force for the active model, which solved the problem that many snake models could not provide a better capture range and evolution stop mechanism. Khokhar *et al.* [18] introduced the characteristic energy function of curvature into the standard level set function, which improved the ability of curve evolution and required fewer iterations.

The tracking methods usually include the definition of seed points and the image derived constraints to guide the growth process. Zhou *et al.* [19] adopted a fuzzy recognition method based on multi-features to guide the probabilistic tracking operator to track along the vessel tree and to measure the vessel axis and diameter while tracking. Later, they introduced the blood vessel structure recognition operator and the blood vessel tracking operator into the fuzzy inference recognition of blood vessels to realize the tracking of blood vessel bifurcations [20].

The graph-based method is a method of mapping the entire image into a graph. One of the classic graph cut segmentation algorithms performs segmentation by solving the energy function minimization problem. Hernandez-Vela *et al.* [21] used graph cut energy function for global optimization when extracting centerline and performing radius measurement. This method is very convenient, but the time complexity and space complexity are high in the calculation. Another commonly used method is the random walk algorithm. The vascular random walk method proposed by Mhiri *et al.* [22] combined Hessian enhancement with random walk and required a manual selection of seed points for segmentation.

The method based on deep learning is to convert the segmentation problem into a classification problem, which is the most widely used segmentation method in recent years. Nasr-Esfahani *et al.* [23] introduced the canny edge detector into training, combining global information with local information using the CNN network. Yang *et al.* [24] added an image mask channel to the CNN single-channel, and the dual-channel processing was more effective in removing catheter regions and artifacts. Jo *et al.* [25] proposed a selective feature mapping method for segmenting the left front descending trunk in cardiovascular images. Fan *et al.* [26] used both the image mask information before angiography and the blood vessel information after angiography as multi-channel input to enhance the structure information of blood vessels, and also matched the mask image with the blood vessel image to obtain a more accurate aligning effect.

All the segmentation methods mentioned above are based on global images and are non-interactive. In practical segmentation and accurate measurement application, it is not the whole blood vessel tree that needs to be concerned and segmented, but one or several of the blood vessel segments of interest. When operators use the segment results obtained by the above methods, they need to select an interest region, and sometimes they need to re-delineate the edge of the segment results due to the not ideal results caused by under-segmentation or over-segmentation. This is equivalent to two steps: a non-interactive automatic segmentation, and a subjective interactive result correction, which is less direct and less efficient. In order to improve the utilization efficiency of clinical data, reduce information redundancy, and reduce time consumption, only segmenting the vessel segment of interest is sufficient to meet the needs of clinical use. Therefore, we propose an interactive segmentation method specifically for the vessels of interest in this paper. This method combines the two steps together by letting the operator perform interactive segmentation directly and the interactive operation is less time-consuming.

For the need for assessing vessels, the diameter of the blood vessel should be measured after segmentation. There are two main approaches to measure the vessel diameter: profile analysis and model establishment. The profile analysis method is based on the different distribution of the gray value of the cross-section of the blood vessel. Zhou *et al.* [27]

studied the distribution of the gray value of the cross-section of the blood vessel according to the 1-D Gaussian matching function, and then the diameter of the blood vessel can be determined according to the characteristics of the Gaussian matching function. After that, Lowell *et al.* [28] developed a 2-D Gaussian differential filter to study the grayscale distribution of blood vessels, so that the measurement effect is better in line with our requirements. The model building method is to analyze the characteristics of blood vessels, so as to establish a suitable mathematical model to simulate the distribution of blood vessels. Al-Diri *et al.* [29] used the contour model to detect the two edges of the blood vessel. The accuracy of the algorithm reached the sub-pixel level. In order to measure the diameter of the blood vessel directly and quickly after segmentation, we use the edge intersection method, which is suitable for our segmentation algorithm.

The rest of this paper is organized as follows: In Section 2, the materials needed and the methods used are introduced. Then, in Section 3, we give a detailed description of the experiment to evaluate our method. Then Section 4 shows the results and discussion of the experiment. Finally, we conclude the paper in Section 4.

II. MATERIALS AND METHODS

A. DATA PREPARATION

The Coronary angiographic images are obtained by means of the angiographic apparatus. All the data-getting processes were carried out in accordance with the approved guidelines and regulations. Since there are no public data sets for cardiovascular angiographic images, a total of 50 representative DICOM sequences were chosen from Siemens AXIOM-Artis by three experienced cardiologists. Then 50 representative slices were picked out and saved as JPG images for subsequent segmentation experiments. The size of all images is 512*512. All the cases and patient information were anonymized.

B. THE SEGMENTATION OF VASCULAR SEGMENTS OF INTEREST

Traditional non-interactive image processing methods are generally used to process the entire picture. In this paper, we use an interactive segmentation method to process blood vessels. Intelligent Scissors algorithm [30], which is also called the Live-Wire algorithm, is an interactive segmentation method for image edge extraction and image composition proposed by Barrett and Mortensen. By adequately constructing the cost function, users can easily and accurately extract the edge of ROI (Region of Interest) in the image based on dynamic programming. The Intelligent Scissors segmentation algorithm transforms the image segmentation problem into a graph search problem that can be solved by the Dijkstra algorithm. Martensen and Barrett [31] believe that Image Local Cost is the basis for image boundary extraction. They use the weighted sum of six image feature values as Image Local Cost. These six feature values are Laplacian zero-crossing, gradient magnitude, gradient direction, Edge pixel value, ''Inside'' pixel value, and ''Outside'' pixel value. And they use different weightings to combine the advantages of various image feature values. Their local cost function is defined as Equation 1.

$$\begin{aligned} l(\boldsymbol{p},\boldsymbol{q}) = {} & w_{\mathrm{Z}} \cdot f_{\mathrm{Z}}(\boldsymbol{q}) + w_{\mathrm{G}} \cdot f_{\mathrm{G}}(\boldsymbol{q}) \\ & + w_{\mathrm{D}} \cdot f_{\mathrm{D}}(\boldsymbol{p},\boldsymbol{q}) + w_{\mathrm{P}} \cdot f_{\mathrm{P}}(\boldsymbol{q}) \\ & + w_{\mathrm{I}} \cdot f_{\mathrm{I}}(\boldsymbol{q}) + w_{\mathrm{O}} \cdot f_{\mathrm{O}}(\boldsymbol{q}) \end{aligned} \tag{1}$$

The more features are included in the calculation process, the more time will be to create the cost map. Therefore, if we use these six image feature values, the increased time is not directly proportional to the effect of improving performance. Thus we choose two most effective image features to calculate image feature values, one is the Canny and the other one is the Gradient Magnitude. Only two image feature values can significantly improve the efficiency of creating the cost map.

The cost function of the image is:

$$C(\boldsymbol{p}) = w_C \cdot f_C(\boldsymbol{p}) + w_G \cdot f_G(\boldsymbol{p}) \tag{2}$$

where $\boldsymbol{p}$ is a pixel in the image, $C(\boldsymbol{p})$ is the cost function of the corresponding edge of pixel $\boldsymbol{p}$. w_C and w_G are the weighting coefficients of the cost function. They are all positive numbers greater than 0, and $w_C + w_G = 1$. $f_C(\boldsymbol{p})$ is the Canny feature function, and $f_G(\boldsymbol{p})$ is the gradient magnitude function. We define the Canny function of the cost function by using the nonlinear mapping of $C(\boldsymbol{p})$. Its definition is shown as Equation 3. The definition of $f_G(\boldsymbol{p})$ is the same as the definition in [31], its definition is shown as Equation 4.

$$f_C(\boldsymbol{p}) = \exp\left\{-4 \times [C(\boldsymbol{p})]^2\right\} \tag{3}$$

$$f_G(\boldsymbol{p}) = 1 - \frac{G(\boldsymbol{p})}{\max(G)} \tag{4}$$

where $C(\boldsymbol{p})$ indicates the Canny value of the pixel $\boldsymbol{p}$, $G(\boldsymbol{p})$ indicates the gradient amplitude. Then the image segmentation problem can convert to the shortest path seeking problem. First select an initial pixel point a on the edge of the blood vessel of interest, then select a pixel point b along the edge of the blood vessel. The path between the two coordinate points displays in real-time. If this path fits well with the edge of the blood vessel, continue to select the next pixel. The pixel point b will be the new starting point just like the initial point a. Repeat the above operation. Otherwise, cancel the pixel point b, reselect a pixel point c, and repeat the above operation until the entire vessel segment of interest is segmented out.

C. OBTAINING THE CENTERLINE OF BLOOD VESSELS

Zhang-Suen is a fast-parallel thinning algorithm widely used in image processing. Zhang's thinning algorithm has the advantages of fast speed, maintaining the connectivity of the thinned curve and no glitch generation, but the result of its thinning cannot guarantee that the curve texture is a single pixel, and the thinning is not thorough.

For the convenience of description, here are some basic concepts:(1) target point and background point: The target point refers to a point with a pixel value of 1, corresponding to the background point with a pixel value of 0.

(2) 8 neighborhoods: as shown in Figure 1, there is an arbitrary pixel point $P1$, and the 8 neighborhoods of $P1$ are the 8 points from $P2$ to $P9$ in the 3×3 region centered on P1 except for $P1$.

P9	P2	P3
P8	P1	P4
P7	P6	P5

FIGURE 1. 8 neighborhoods of P1.

(3) Boundary point: belongs to the target point, and at least one of its 8 neighborhoods is the background point.

(4) End point: belongs to the boundary point, and at least one of its 8 neighbors is the target point.

Set the target point as value 1 and the background point as value 0. Zhang's fast parallel thinning algorithm execution process performs the following operations on the boundary points:

1) Find 8 neighborhoods centered on the boundary point,and mark the center point as $P1$. The 8 neighborhood points are clockwise around the center point are $P2$,$P3$, . . . , $P9$ respectively, where $P2$ is above $P1$. Mark the boundary points that meet the following conditions:

$$2 \leq N(P1) \leq 6 \tag{5}$$

$$S(P1) = 1 \tag{6}$$

$$P2 \times P4 \times P6 = 0 \tag{7}$$

$$P4 \times P6 \times P8 = 0 \tag{8}$$

where $N(P1)$ is the number of non-zero neighbors of $P1$, and $S(P)$ is the number of times the values of these points change from 0 to 1 when $P2$,$P3$, . . . , $P9$ are in order.

2) As in step 1, one changes the previous condition (7) to (9) and condition (8) to (10). Similarly, after checking all the boundary points, remove all the marked ones.

$$P2 \times P4 \times P8 = 0 \tag{9}$$

$$P2 \times P6 \times P8 = 0 \tag{10}$$

3) The above two steps constitute an iteration until no points meet the marking conditions, and then the remaining points compose the area of the thinned skeleton.

Only using the Zhang-Suen thinning algorithm, the resulting centerline may be bifurcated or causing non-single pixels somewhere, such as Figure 2.

In order to solve the possible bifurcation problem and the non-single-pixel problem of the centerline, we improve the Zhang-Suen thinning algorithm. After analyzing the principle of the Zhang thinning algorithm and the thinned image, it is found that the cause of the non-single pixels in the thinned texture is that some of the deleted points are omitted because they do not meet the deletion conditions (6). We divide these points into three categories.

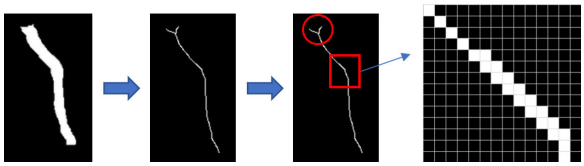

FIGURE 2. Bifurcation and non-single pixel after thinning.

The first category is that the number of target pixels in 8-neighborhood points is 2, and there are four types in total, as shown in Figure 3.

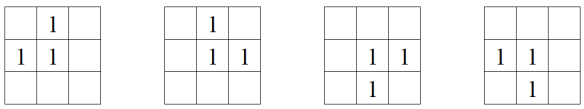

FIGURE 3. Four types of the first category.

The second category is that the number of target pixels in 8-neighborhood points is 3, and there are eight types in total, as shown in Figure 4.

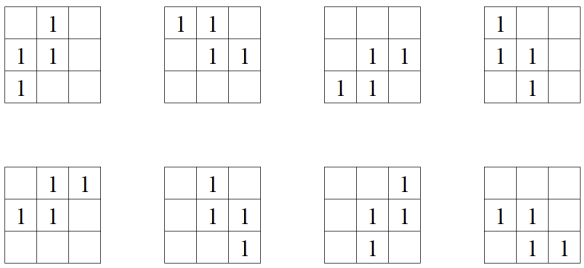

FIGURE 4. Eight types of the second category.

The third category is that the number of target pixels in 8-neighborhood points is 4, and there are four types in total, as shown in Figure 5.

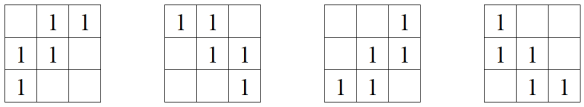

FIGURE 5. Four types of the third category.

In order to identify these points easily, we encode 8 neighborhood points from $P2$ to $P9$, a one-bit binary number represents each bit. If the neighborhood point value is 1, the corresponding binary bit is 1, if the neighborhood point value is 0, the corresponding binary bit is 0, as shown in Figure 6.

Encode all 8 neighbors of target points that may be missed in thinning and convert them to decimal. The conversion results of the first category points are: 65, 5, 20 and 80, and

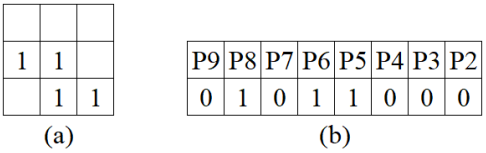

FIGURE 6. (a) is the 8 neighborhoods of the target point, and (b) shows the binary code after the encoding.

the conversion results of the second category points are: 133, 52, 208, 67, 13, 22 and 88, the conversion results of the third category points are: 99, 141, 54 and 216. In the process of thinning, we use Equation 11 to compute the binary encoding $B(P1)$ of all the eight neighboring regions of the target points and delete the target points if $B(P1)$ belongs to the 16 target points mentioned above.

$$B(P1) = \sum_{n=2}^{9} \left(Pn \times 2^{n-2} \right) \tag{11}$$

Compared with the original Zhang thinning algorithm, we use condition (12) instead of condition (6) to judge whether the target point needs to be deleted.

$$S(P1) = 1 \; OR \; B(P1) \in \{65, 5, 20, 80, 97, 133, 52, 208, 67, 13, 22, 88, 99, 141, 54, 216\} \tag{12}$$

In this fashion, the skeleton points on the centerline of the blood vessel obtained by thinning are all single pixels, thus resulting in a more accurate vessel diameter measurement method.

D. MEASUREMENT OF VESSEL DIAMETER

In this paper, we propose a new method for the measurement of the vessel diameter. Figure 7 presents the flow chart of this method.

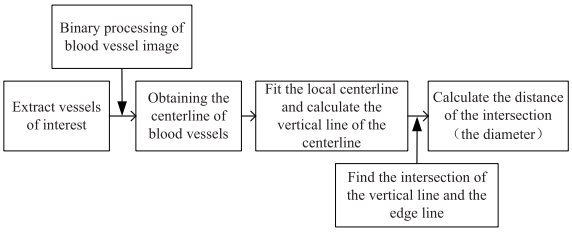

FIGURE 7. Work-flow of diameter measurement of the vessel of interest.

According to the obtained centerline fitting line, we can find its vertical line, which should be perpendicular to the two edge lines from the local consideration, so that its intersections with the two edge lines can represent the diameter of the blood vessel at that point, as shown in Figure 8.

In order to ensure the smooth change of the slope of the centerline, for each point Pi on the centerline, choose m points before and after the Pi point, and use the least-squares approximation method to fit the straight line. Suppose the line to be fitted is $y = ax + b$, for each data point

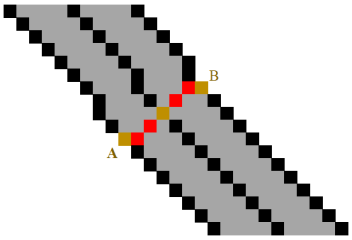

FIGURE 8. Schematic diagram of blood vessel diameter.

$P_i(x, y), i = 1, 2, \ldots, m$ we can calculate the approximate value by fitting the straight line equation, recorded as y. The idea of least squares is to minimize the sum of squared residuals between the measured value and the approximate value, which means to minimize Equation 13 as much as possible.

$$D = \sum_{i}^{n} (y_i - b - ax_i)^2 \tag{13}$$

The derivation shows that Equation 13 can reach the minimum value when Equation 14 and Equation 15 are satisfied.

$$a = \frac{n \sum_{i=1}^{n} x_i y_i - \sum_{i=1}^{n} x_i \sum_{i=1}^{n} y_i}{n \sum_{i=1}^{n} x_i^2 - \left(\sum_{i=1}^{n} x_i \right)^2} \tag{14}$$

$$b = \frac{\sum_{i=1}^{n} x_i^2 \sum_{i=1}^{n} y_i - \sum_{i=1}^{n} x_i \sum_{i=1}^{n} x_i y_i}{n \sum_{i=1}^{n} x_i^2 - \left(\sum_{i=1}^{n} x_i \right)^2} \tag{15}$$

As shown in FIGURE 8, the digital image is discrete, and the vertical line passing through the centerline does not necessarily intersect the edge, so the edge point closest to the vertical line is taken as the endpoint of the blood vessel diameter at both ends.

Point A and point B are intersections. Assuming that the coordinates of the intersection are $A\,(x_a, y_a)$ and $B\,(y_a, y_b)$, then the diameter of the blood vessel at the center point is (16).

$$d = \sqrt{(x_a - x_b)^2 + (y_a - y_b)^2} \tag{16}$$

III. EXPERIMENTAL DESIGN

A. SEGMENTATION OF VASCULAR SEGMENTS OF INTEREST

1) PARAMETER SETTING AND DATA PREPARATION

To verify the performance of our proposed method, we make an experiment to compare the results of different methods based on the same images. We implemented the u-net method [32] as method 1 and the classical multi-scale Hessian method [33] as method 2. In our improved intelligent scissors algorithm, we define $w_C = 0.45$, $w_G = 0.55$, which has been proved to have good effects on most images.

We performed method 1 and method 2 on the 50 vessel images to get segmentation results of both methods. The foreground of the results is white while the background is black. And all the selected 50 vessel images were manually delineated and segmented using PhotoShop software by the

cardiologists. Then we process binary processing to get vessel images in which the background is black, while the foreground is white as our ground truth.

In order to evaluate the performance of segmenting specific vessel segments, we only compare the segmentation results of vessel segments of interest area rather than the global segmentation results. We designed a batch processing program in which cardiologists draw a rectangle on the original image to select the blood vessels of interest and get a source image mask with the same size as the original image. Only the part inside the rectangle exists in the source image mask. The background outside the rectangle is black. The segmentation results of method 1, method 2, and ground truth will also be performed with the same mask creating operations in the same rectangular position to get the mask of method 1, method 2, and ground truth respectively at the same time. Our method is applied to the original image mask to get our segmentation results with a white foreground and a black background. Then the masks of method 1, method 2, and our segmentation results will be compared with the source image mask respectively to evaluate the segmentation performance.

2) PERFORMANCE METRICS

We use five different performance measures to compare our segmentation results with other methods. The five performance measures are as follows: Dice Similarity Coefficient (DSC), Sensitivity (Recall), Precision, Specificity, Jaccard Similarity (JAC), and Hausdorff distance (HD). To calculate these performance measures, the true positive (TP), the true negative (TN), the false positive (FP), and the false negative (FN) need to be computed firstly. TP, FN, FP, and TN denote true positive (the vessel pixels correctly identified), false negative (the vessel pixels that are not identified), false positive (the non-vessel pixels that are wrongly identified as vessel pixels), and true negative (the non-vessel pixels correctly identified) respectively.

Dice coefficient(DSC):

$$DSC = \frac{2 \times TP}{(FP + TP) + (TP + FN)} \tag{17}$$

Sensitivity(Recall):

$$Sensitivity = \frac{TP}{TP + FN} \tag{18}$$

Precision:

$$Precision = \frac{TP}{TP + FP} \tag{19}$$

Specificity:

$$Specificity = \frac{TN}{TN + FP} \tag{20}$$

Jaccard similarity:

$$JAC = \frac{TP}{FP + TP + FN} \tag{21}$$

Hausdorff distance:

$$\begin{aligned} d_H(X, Y) &= \max |d_{XY}, d_{YX}| \\ &= \max \left\{ \max_{x \in X} \min_{y \in Y} d(x, y), \max_{y \in Y} \min_{x \in X} d(x, y) \right\} \end{aligned} \tag{22}$$

The greater the DSC is, the higher the degree of overlap between the target vessel and the actual vessel segmented by the segmentation method. JAC is used to compare the similarity and differences between limited sample sets. If the JAC coefficient is larger, it means that their similarity is higher.

Sensitivity(Recall) means correctly detected positive parts, while Specificity means correctly detected negative parts. If the Sensitivity increases, the missed segmentation rate will decrease, and if the Specificity increases, the error segmentation rate will decrease.

Precision is the ratio of the number of correctly predicted parts to the total number of positive predictions, which represents how many predictions are accurate from the perspective of prediction results.

Hausdorff distance is a measure to describe the similarity between two sets of points. The smaller the value is, the better the segmentation result is.

B. SUBJECTIVE EVALUATION OF DIAMETER MEASUREMENT

The cardiovascular diameter measurement is mainly used to analyze the degree of stenosis of blood vessels. The changing trend and stenosis of the blood vessels can be seen intuitively. We select two representative blood vessel segments for qualitative analysis, one of which is a common blood vessel segment with a slight change in thickness, and the other is a diseased blood vessel segment with stenosis, to verify whether our method of measuring diameter can have an excellent measuring effect.

C. QUANTITATIVE EVALUATION OF DIAMETER MEASUREMENT

Since we cannot directly measure the diameter of a real blood vessel, in order to measure the accuracy of the diameter measurement, we constructed some specially set benchmarks that know the specific width. These benchmarks are used to verify the accuracy of diameter measurements. We design 12 benchmarks with similar blood vessel curvature and similar width, as shown in Figure 9.

The effect of diameter measurement can be evaluated by comparing the average and standard deviation of the diameter measurement results and the real values of these 12 benchmarks.

IV. RESULTS AND DISCUSSION

A. RESULTS OF SEGMENTATION OF VASCULAR SEGMENTS OF INTEREST

Figure 10 shows the process of segmentation of the vessel segment of interest. After setting the starting point on the marked endpoint, set the target point to form a connecting

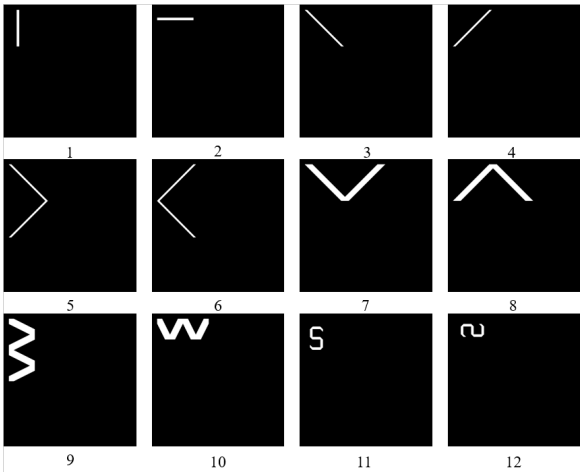

FIGURE 9. Schematic diagram of 12 benchmarks.

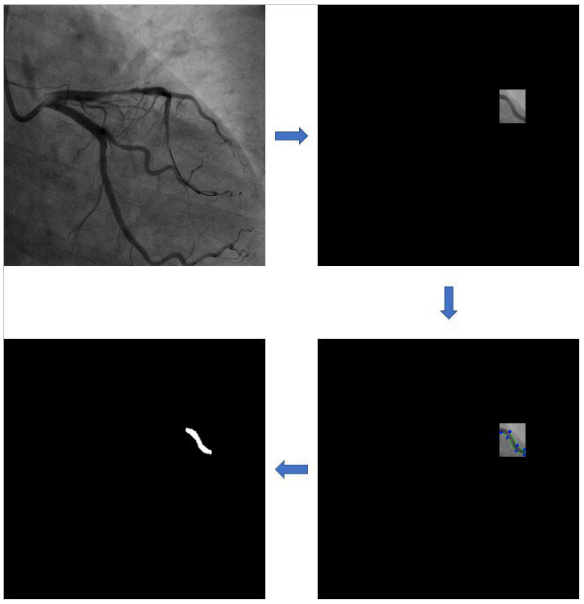

FIGURE 10. Schematic diagram of segmentation of vascular segments.

line continuously. The seed point with weak effect can be deleted and reset. The process of segmentation does not end until the obtained path forms a closed area to complete the segmentation.

We evaluated the performance of the segmentation results of 50 vessel segments using the masks of method1, masks of method2, ground truth masks, and segmentation results of our method. The results are shown in Figure 11. From Figure 11, the AUC value of our method is larger than the others, and it reaches 0.9919.

In order to evaluate the performance of the segmentation algorithm in more detail, we separately calculated DSC, Sensitivity, Precision, Specificity,Jaccard index, Hausdorff distance of every vessel segment. Figure 12 shows box plots for overall DSC, Sensitivity, Precision, Specificity, JAC, and HD for method1, method2, and our method, respectively.

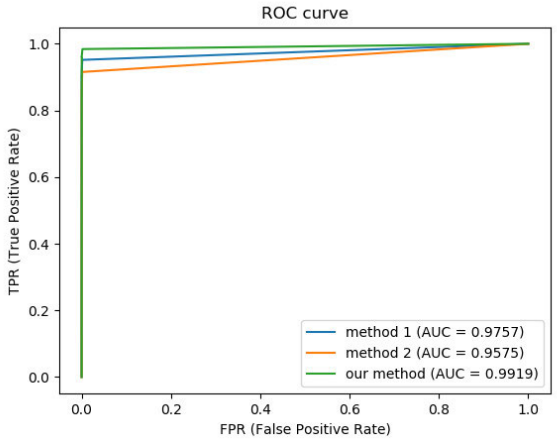

FIGURE 11. ROC curve and AUC values of three methods.

The red line in the box represents the median value and the red cross represents an outlier. It is obvious to observe that method 1 and method 2 have more outliers than our method, which means that method 1 and method 2 are not such stable in practical vessel segment segmentation progress. In order to achieve a stable effect, methods 1 and 2 need to introduce some interactive operations to make some corrections in some under-segmentation or over-segmentation areas.

Table 1 shows the average DSC, Sensitivity, Precision, Specificity, JAC, and HD of three methods of 50 vessel segments. These data indicate that the segmentation with our segmentation method can obtain good segmentation results. The average DSC, Sensitivity, JAC, and HD are better than the other two methods. Precision is the positive predictive value. It is influenced by *TP* and *FP* according to Equation 19. The larger *FP* is, the smaller the Precision is. As our method is based on discrete single pixels when delineating the boundary, it may cause the segment results to have jagged borders that contain real curve borders. To improve this, some curve fitting of the jagged border can be done in the future. Meanwhile, the better the feature is selected and the cost function is constructed, the better the segmentation effect of the edge will be during segmentation.

TABLE 1. Average DSC, Sensitivity, Precision, Specificity, JAC, and HD of three methods of 50 vessel segments.

Method	DSC	Sensitivity	Precision	Specificity	JAC	HD
Method 1	0.8883	0.8563	0.9355	0.9998	0.8045	7.8117
Method 2	0.9176	0.8921	0.9602	0.9999	0.8583	3.9627
Our method	0.9255	0.9534	0.9020	0.9997	0.8622	2.7107

B. RESULTS OF THE DIAMETER MEASUREMENT SUBJECTIVE EVALUATION

We chose healthy blood vessels as blood vessel segment I, and blood vessels with stenosis as blood vessel segments II. Then we get their centerline after the thinning process, respectively, as shown in Figure 13 and Figure 15.

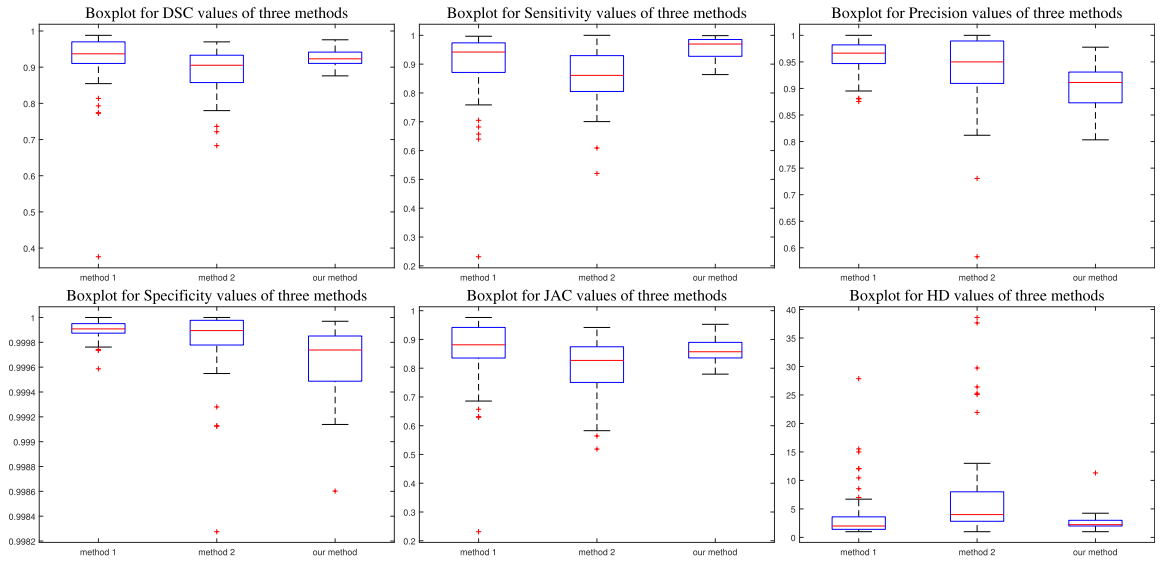

FIGURE 12. Boxplot for six metircs values of three methods.

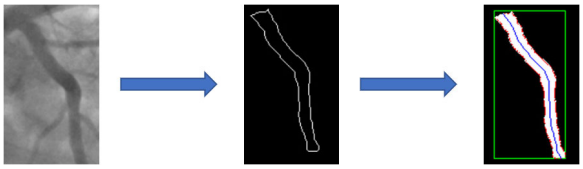

FIGURE 13. Extraction result of centerline of vascular segment I.

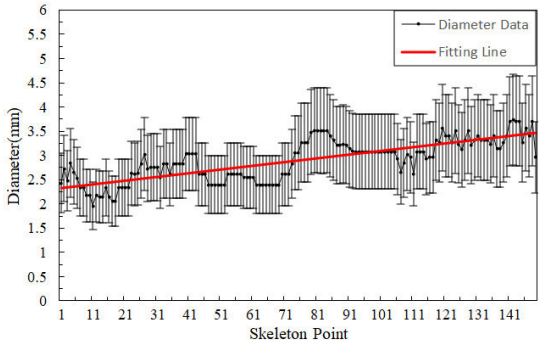

FIGURE 14. Diagram of diameter measurement error of vascular segment I.

Figure 13 is the result of the extraction of the centerline of segment I. A two-dimensional skeleton of 149 discrete points is obtained. Obtain the diameter of each skeleton point by calculating the distance between the two intersections of the vertical line and the edge of the blood vessel. The calculated measurement error is shown in Figure 14. The abscissa is the skeleton point, and the ordinate represents the two-dimensional diameter (unit: mm).

Since the length of the blood vessel diameter directly obtained is measured by the number of pixels, in order to more intuitively and accurately reflect the actual blood vessel

FIGURE 15. Extraction result of centerline of vascular segment II.

diameter, we convert the length by referring to the pixel spacing information in the DICOM TAG, The pixel spacing of Figure 13 and Figure 15 is 0.308. The ordinate is the result obtained after conversion. As we can see, the trend of the fitting line in Figure 14 can reflect the actual change of blood vessels, and the 2-3 mm shown in the ordinate value is also in accordance with the standard cardiovascular diameter of the human body.

Figure 15 is the result of the extraction of the centerline of segment II. A two-dimensional skeleton of 74 discrete points is obtained. Similarly, its calculated measurement error is shown in Figure 16. Intuitively, it can be seen from Figure 15 that there is stenosis in the segment II of the blood vessel, which corresponds to the apparent depression of the blood vessel at the 35th skeleton point in the diameter curve of Figure 16. This method of measuring and analyzing the diameter of blood vessels can be used to diagnose the presence of coronary artery stenosis, initially.

C. QUANTITATIVE ANALYSIS AND STATISTICS OF VESSEL DIAMETER

For each benchmark, the centerline is first obtained by thinning operation. Manually mark the diameter of the blood vessel corresponding to each centerline, and then calculate the diameter according to the coordinates of the first and last points of the mark, as the real blood vessel diameter. The real diameter values and the diameter measurement values are compared, as shown in Figure 17. This is the comparison chart of the real diameter and the diameter measurement of

TABLE 2. Error table of all benchmarks.

Image number	Skeleton points	Real diameter(unit:pixel)		Measurement of algorithm(unit:pixel)	
		Mean	Standard deviation	Mean	Standard deviation
1	140	9.00000	0.00000	9.05539	0.00000
2	140	9.00000	0.00000	9.06085	0.04119
3	137	5.65685	0.00000	5.63833	0.07170
4	137	5.65685	0.00000	5.65158	0.06930
5	276	5.69554	0.34983	5.65777	0.08794
6	276	5.69882	0.35843	5.70656	0.39511
7	267	19.72292	0.64943	19.71940	0.65455
8	265	19.68305	0.61442	19.67640	0.62014
9	369	25.07001	0.93849	25.07520	1.93849
10	279	24.96774	0.38287	24.83080	1.44195
11	185	8.44468	0.14405	8.53869	1.27082
12	185	8.48189	0.23602	8.56095	1.28055

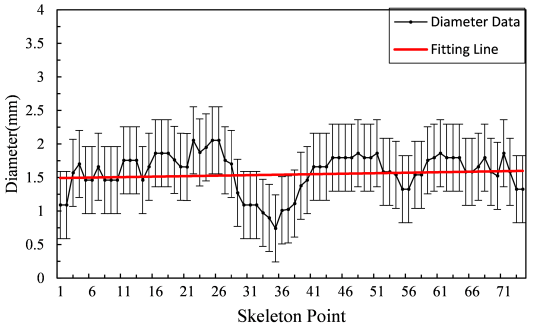

FIGURE 16. Diagram of diameter measurement error of vascular segment II.

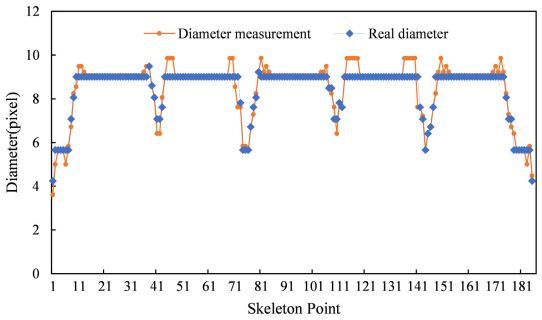

FIGURE 17. Comparison chart between real diameter and diameter measurement.

the benchmark 11. The abscissa is the serial number of the bone point, while the ordinate is the length value of which the unit is the pixel. We can see that the two curves coincide, indicating that the measured value is close to the real value.

The statistical results of the actual and measured values of the 12 benchmarks are shown in Table 2. It can be seen from Table 2 that the measurement result of the blood vessel without direction change is very close to the actual value, and the measurement result does not fluctuate much, indicating that the measurement result has high accuracy. For blood vessels with direction changes, the result is closer to the actual value, and the standard deviation is slightly higher than the actual value.

Since the digital image is discrete, the diameter is calculated using the coordinates of two pixels. However, more often, the vertical line with the centerline normal does not pass directly through the coordinate points on the two edges. Instead, the point on the edge that is close to the perpendicular is chosen. This situation can cause some errors, especially if the blood vessels are small or if the direction of the blood vessels changes. These errors cannot be avoided. As long as the measurement results can accurately reflect the trend of the blood vessel and the width of the blood vessel within the acceptable error range, it can be regarded as a proper blood vessel diameter measurement method.

D. EXPERIMENTAL PLATFORM AND TIME CONSUMPTION

All experiments were conducted on a standard PC (AMD Ryzen 7 7200X Eight-Core Processor @ 3.70 GHz, processor with 8 GB of RAM, Windows 10 64-bit). The algorithm was implemented in Visual Studio 2017. We calculated the average value of the total time of segmentation, thinning, and diameter measurement of all the 50 vessel segments. The average value was 12.6s. The time consumption of interactive segmentation operation is related to the proficiency of the operator.

V. CONCLUSION

The aim of our research was to propose an interactive method specifically for the extraction of blood vessel regions of interest and a method for measuring the diameter of blood vessels corresponding to this kind of segmentation method. Considering that the commonly used global-based image segmentation methods lack particular pertinence and are somewhat redundant for its global operations, the most inconvenient is that the results obtained need to be manually confirmed. We use manual interactive segmentation to reduce redundancy, and it is equivalent to putting the manual confirmation process into the segmentation process. All the segmentation results are compared with ground truths, which were explicitly manually segmented by experienced cardiologists. The average Dice Similarity Coefficient (DSC), Sensitivity, Precision, Specificity, Jaccard Similarity (JAC), and Hausdorff distance (HD) are 0.9255, 0.9534, 0.9020, 0.9997, 0.8622 and

2.7107 respectively. These results indicate that the segmentation works well. However, this segmentation method also has limitations, and it is difficult to operate for small blood vessel parts and bifurcations. Corresponding pre-processing operations can be added to increase the contrast between the blood vessel part and the background before the segmentation operation. Future work is to improve the cost function and extract more effective features to continuously optimize the effect of segmentation.

We use the edge intersection method for the diameter measurement on the segmentation result. First, thin the result after segmentation to obtain the centerline, and then obtain the intersection points of the vertical line of the centerline normal and the edges of the blood vessel. The distance between the two intersection points is the diameter. We conducted a qualitative and quantitative assessment of the diameter measurement, and the results confirmed that the diameter measurement results could reflect the thickness of the blood vessel. However, because the digital image is discrete, the deviation of a pixel selection will cause the deviation of the value. For small blood vessels, this value has a significant influence. Therefore, the effect of measuring the diameter of small blood vessels is unstable. How to improve the diameter measurement effort of small blood vessels is what needs to be solved in the future.

REFERENCES

[1] I. Khan, "An introduction to computer viruses: Problems and solutions," *Library Hi Tech News*, vol. 29, no. 7, pp. 8–12, Sep. 2012.
[2] H. A. Kirişli *et al.*, "Standardized evaluation framework for evaluating coronary artery stenosis detection, stenosis quantification and lumen segmentation algorithms in computed tomography angiography," *Med. Image Anal.*, vol. 17, no. 8, pp. 859–876, Dec. 2013.
[3] S. Moccia, E. De Momi, S. El Hadji, and L. S. Mattos, "Blood vessel segmentation algorithms—Review of methods, datasets and evaluation metrics," *Comput. Methods Programs Biomed.*, vol. 158, pp. 71–91, May 2018.
[4] C. Kirbas and F. Quek, "A review of vessel extraction techniques and algorithms," *ACM Comput. Surv.*, vol. 36, no. 2, pp. 81–121, Jun. 2004.
[5] K. Sun, "Development of segmentation methods for vascular angiogram," *IETE Tech. Rev.*, vol. 28, no. 5, p. 392, 2011.
[6] Y. Lian, Y. Wang, J. Yu, Y. Guo, and L. Chen, "Segmentation of arteriovenous malformations nidus and vessel in digital subtraction angiography images based on an iterative thresholding method," in *Proc. 8th Int. Conf. Biomed. Eng. Informat. (BMEI)*, Oct. 2015, pp. 111–115.
[7] I. Cruz-Aceves, F. Oloumi, R. M. Rangayyan, J. G. Aviña-Cervantes, and A. Hernandez-Aguirre, "Automatic segmentation of coronary arteries using Gabor filters and thresholding based on multiobjective optimization," *Biomed. Signal Process. Control*, vol. 25, pp. 76–85, Mar. 2016.
[8] S. Wang, B. Li, and S. Zhou, "A segmentation method of coronary angiograms based on multi-scale filtering and region-growing," in *Proc. Int. Conf. Biomed. Eng. Biotechnol.*, May 2012, pp. 678–681.
[9] K. A. S. H. Kulathilake, L. Ranathunga, G. R. Constantine, and N. A. Abdullah, "Region growing segmentation method for extracting vessel structures from coronary cine-angiograms," in *Proc. Moratuwa Eng. Res. Conf. (MERCon)*, Apr. 2015, pp. 142–147.
[10] A. Kerkeni, A. Benabdallah, A. Manzanera, and M. H. Bedoui, "A coronary artery segmentation method based on multiscale analysis and region growing," *Comput. Med. Imag. Graph.*, vol. 48, pp. 49–61, Mar. 2016.
[11] R. Nock and F. Nielsen, "Statistical region merging," *IEEE Trans. Pattern Anal. Mach. Intell.*, vol. 26, no. 11, pp. 1452–1458, Nov. 2004.
[12] T. Wan, X. Shang, W. Yang, J. Chen, D. Li, and Z. Qin, "Automated coronary artery tree segmentation in X-ray angiography using improved Hessian based enhancement and statistical region merging," *Comput. Methods Programs Biomed.*, vol. 157, pp. 179–190, Apr. 2018.
[13] S. Chaudhuri, S. Chatterjee, N. Katz, M. Nelson, and M. Goldbaum, "Detection of blood vessels in retinal images using two-dimensional matched filters," *IEEE Trans. Med. Imag.*, vol. 8, no. 3, pp. 263–269, Sep. 1989.
[14] I. Cruz-Aceves, F. Cervantes-Sanchez, and M. S. Avila-Garcia, "A novel multiscale Gaussian-matched filter using neural networks for the segmentation of X-ray coronary angiograms," *J. Healthcare Eng.*, vol. 2018, pp. 1–11, Apr. 2018.
[15] M. Kass, A. Witkin, and D. Terzopoulos, "Snakes: Active contour models," *Int. J. Comput. Vis.*, vol. 1, no. 4, pp. 321–331, Jan. 1988.
[16] S. Osher and J. A. Sethian, "Fronts propagating with curvature-dependent speed: Algorithms based on Hamilton–Jacobi formulations," *J. Comput. Phys.*, vol. 79, no. 1, pp. 12–49, Nov. 1988.
[17] S. N. Devi and N. Kumaravel, "Comparison of active contour models for image segmentation in X-ray coronary angiogram images," *J. Med. Eng. Technol.*, vol. 32, no. 5, pp. 408–418, Jan. 2008.
[18] M. Khokhar, S. Talpur, S. A. Khowaja, and R. A. Shah, "A novel curvature feature embedded level set method for image segmentation of coronary angiograms," in *Trends and Advances in Information Systems and Technologies* (Advances in Intelligent Systems and Computing). 2018, pp. 831–841.
[19] S. Zhou, J. Yang, W. Chen, and Y. Wang, "New approach to the automatic segmentation of coronary artery in X-ray angiograms," *Sci. China F, Inf. Sci.*, vol. 51, no. 1, pp. 25–39, Jan. 2008.
[20] Z. Shoujun, Y. Jian, W. Yongtian, and C. Wufan, "Automatic segmentation of coronary angiograms based on fuzzy inferring and probabilistic tracking," *Biomed. Eng. OnLine*, vol. 9, no. 1, p. 40, 2010.
[21] A. Hernandez-Vela, C. Gatta, S. Escalera, L. Igual, V. Martin-Yuste, M. Sabate, and P. Radeva, "Accurate coronary centerline extraction, caliber estimation, and catheter detection in angiographies," *IEEE Trans. Inf. Technol. Biomed.*, vol. 16, no. 6, pp. 1332–1340, Nov. 2012.
[22] F. M'hiri, L. Duong, C. Desrosiers, and M. Cheriet, "Vesselwalker: Coronary arteries segmentation using random walks and Hessian-based vesselness filter," in *Proc. IEEE 10th Int. Symp. Biomed. Imag.*, Apr. 2013, pp. 918–921.
[23] E. Nasr-Esfahani, N. Karimi, M. H. Jafari, S. M. R. Soroushmehr, S. Samavi, B. K. Nallamothu, and K. Najarian, "Segmentation of vessels in angiograms using convolutional neural networks," *Biomed. Signal Process. Control*, vol. 40, pp. 240–251, Feb. 2018.
[24] S. Yang, J. Yang, Y. Wang, Q. Yang, D. Ai, and Y. Wang, "Automatic coronary artery segmentation in X-ray angiograms by multiple convolutional neural networks," in *Proc. 3rd Int. Conf. Multimedia Image Process. (ICMIP)*, 2018, pp. 31–35.
[25] K. Jo, J. Kweon, Y.-H. Kim, and J. Choi, "Segmentation of the main vessel of the left anterior descending artery using selective feature mapping in coronary angiography," *IEEE Access*, vol. 7, pp. 919–930, 2019.
[26] J. Fan, J. Yang, Y. Wang, S. Yang, D. Ai, Y. Huang, H. Song, A. Hao, and Y. Wang, "Multichannel fully convolutional network for coronary artery segmentation in X-ray angiograms," *IEEE Access*, vol. 6, pp. 44635–44643, 2018.
[27] L. Zhou, M. S. Rzeszotarski, L. J. Singerman, and J. M. Chokreff, "The detection and quantification of retinopathy using digital angiograms," *IEEE Trans. Med. Imag.*, vol. 13, no. 4, pp. 619–626, Dec. 1994.
[28] J. Lowell, A. Hunter, D. Steel, A. Basu, R. Ryder, and R. L. Kennedy, "Measurement of retinal vessel widths from fundus images based on 2-D modeling," *IEEE Trans. Med. Imag.*, vol. 23, no. 10, pp. 1196–1204, Oct. 2004.
[29] B. Al-Diri, A. Hunter, and D. Steel, "An active contour model for segmenting and measuring retinal vessels," *IEEE Trans. Med. Imag.*, vol. 28, no. 9, pp. 1488–1497, Sep. 2009.
[30] E. N. Mortensen and W. A. Barrett, "Intelligent scissors for image composition," in *Proc. 22nd Annu. Conf. Comput. Graph. Interact. Techn. (SIGGRAPH)*, 1995, pp. 191–198.
[31] E. N. Mortensen and W. A. Barrett, "Interactive segmentation with intelligent scissors," *Graph. Models Image Process.*, vol. 60, no. 5, pp. 349–384, Sep. 1998.
[32] O. Ronneberger, P. Fischer, and T. Brox, "U-net: Convolutional networks for biomedical image segmentation," in *Medical Image Computing and Computer-Assisted Intervention—MICCAI* (Lecture Notes in Computer Science). 2015, pp. 234–241.
[33] Q. Li, S. Sone, and K. Doi, "Selective enhancement filters for nodules, vessels, and airway walls in two- and three-dimensional CT scans," *Med. Phys.*, vol. 30, no. 8, pp. 2040–2051, Jul. 2003.

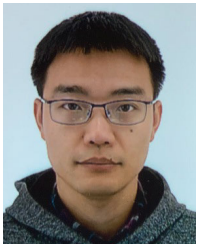

LURONG JIANG received the B.S. degree in electronic communication engineering from Zhejiang University, in 2004, the M.S. degree in control theory and control engineering from Hangzhou Dianzi University, in 2009, and the Ph.D. degree in circuits and systems from Zhejiang University, in 2015. Since 2015, he has been a Lecturer with the School of Information Science and Technology, Zhejiang Sci-Tech University, Hangzhou, China. He currently chairs a National Natural Science Foundation Project. His research interests include signal processing, complex networks, and wireless sensor networks.

YUE LI received the B.S. degree in communication engineering from Zhejiang Sci-Tech University, in 2018, where she is currently pursuing the master's degree in software engineering. Her research interest includes medical image processing.

JIANWEI PAN was born in January 1977. He received the Ph.D. degree in medical science from Zhejiang University, in 2010. He is currently a Clinical Professor with Zhejiang University. He is also a master's Tutor. His research interests include stroke and medical image processing.

DANHUA ZHU was born in December 1980. He received the B.S. and Ph.D. degrees in biomedical engineering from Zhejiang University, in 2003 and 2011, respectively. He is currently a Research Associate with the State Key Laboratory for Diagnosis and Treatment of Infectious Diseases, Zhejiang University. His research interests include medical image and signal processing, embedded systems and instrumentation, brain–computer interface, and artificial liver.

JIJUN TONG was born in September 1977. He received the B.S., M.S., and Ph.D. degrees in biomedical engineering from Zhejiang University, in 1999, 2003, and 2008, respectively. He is currently a Professor with Zhejiang Sci-Tech University. He is also a master's Tutor. His research interests include medical big data, medical image and signal processing, embedded systems and instrumentation, and wireless sensor networks.

TING SHU was born in July 1979. He received the Ph.D. degree in computer science from Zhejiang University, in 2010. He is currently an Associate Professor with the School of Information Science and Technology, Zhejiang Sci-Tech University, Hangzhou, China. His current research interests include software testing and network protocol testing.